Transmission losses of a turbofan inlet duct lined with porous materials

C. Chan, E. Perrey-Debain, J-M. Ville, B. Poirier†

Sorbonne Universités,
Université de Technologie de Compiègne,
Laboratoire Roberval UMR CNRS 7337

† Safran/Snecma, Etablissement Villaroche Sud, Rond-point René Ravaud - Réau, 77550 Moissy-Cramayel, France

SAPEM 2017, Le Mans

utc Recherche Roberval
SORBONNE UNIVERSITES

cnrs

Locally vs non-locally liner

DDOF liner with wire-mesh septum

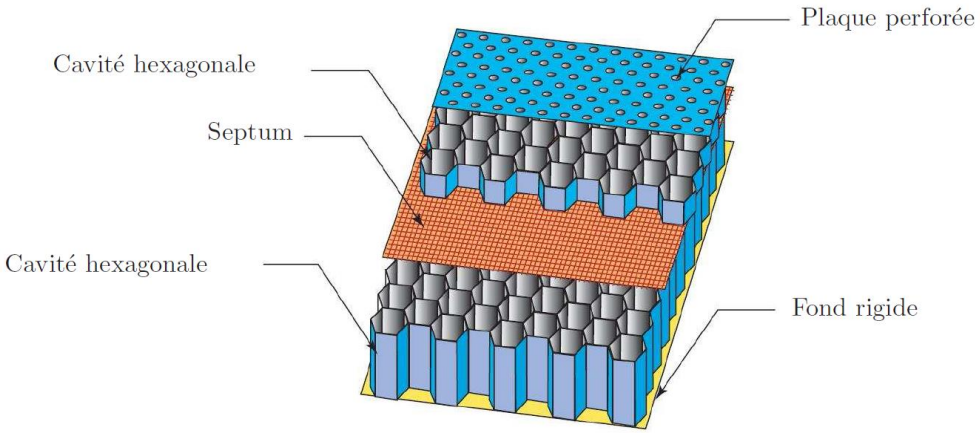

Metal foam

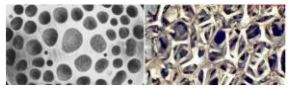

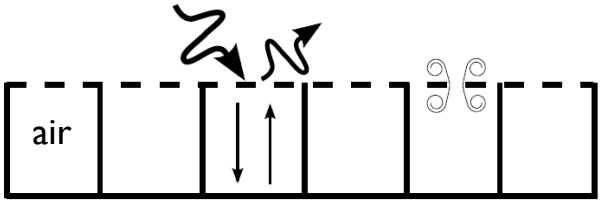

Classical locally reacting liner

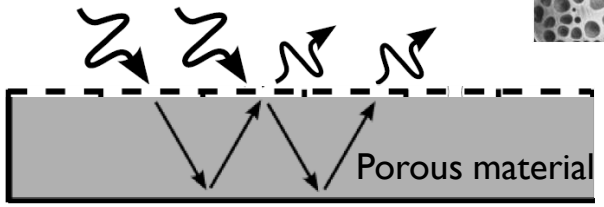

Non-locally reacting liner with porous material and perforate sheet

Modeling the perforate sheet impedance $Z = R + iX$

Yu J, Ruiz M, Kwan HW. Validation of goodrich perforate liner impedance model using NASA langley test data. In: Proceedings of the 14th AIAA/CEAS aeroacoustics conference & exhibit.

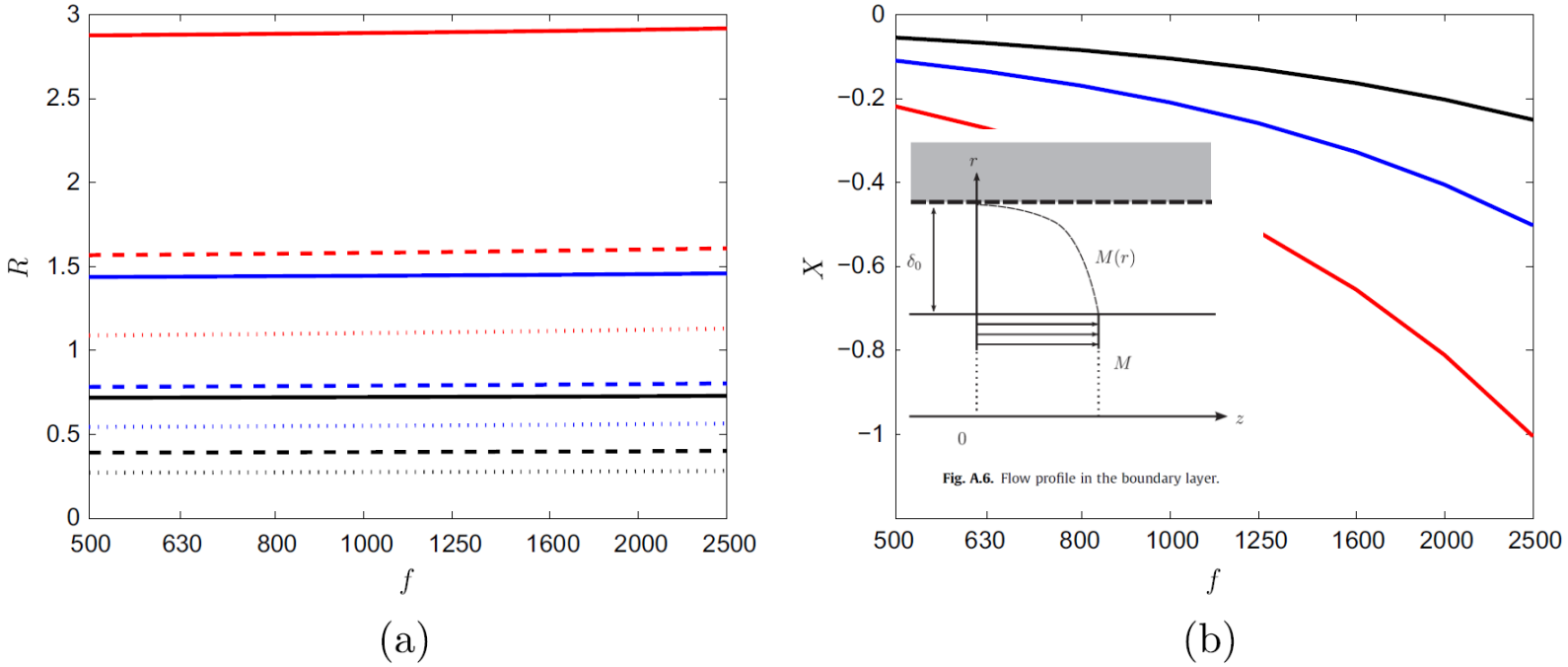

Fig. A.6. Flow profile in the boundary layer.

Fig. A.7. Normalized impedance ((a) resistance and (b) reactance) as a function of the frequency at $M = -0.5$. P1: (——), P2: (——), P3: (——). Solid line: $\delta = 1\%$, dashed line: $\delta = 3\%$, dotted line: $\delta = 5\%$.

Perf. Plate	POA (%)	τ (mm)	d (mm)
P1	20	1	1
P2	10	1	1
P3	5	1	1

Modeling the porous material

$$\rho_e = \frac{\rho_0/\phi}{1 - F\left(\frac{a}{\delta_v}\right)},$$

$$K_e = \frac{\gamma P_0/\phi}{1 - (\gamma - 1)F\left(\sqrt{Pr}\,\frac{a}{\delta_v}\right)},$$

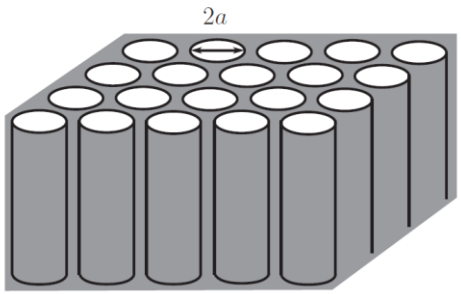

Fig. 2. Schematic of the perforated solid.

where $\delta_v = \left(\frac{2\eta}{\omega\rho}\right)^{1/2}$ is the viscous boundary layer in the pores, a the radius of the pores, η the dynamic viscosity, Pr the Prandtl number, γ the specific heat ratio, ϕ the porosity and F the function

$$F(x) = \frac{2J_1((1+i)x)}{(1+i)xJ_0((1+i)x)}. \tag{28}$$

The approach of Zwikker and Kosten permits to separate the viscous and thermal effects and is valid if $a > 10$ μm and $af^{3/2} < 10^4$ ms$^{-3/2}$ as shown by Stinson [31]. The resistivity of the material is given by

$$\sigma = 8\eta/\phi a^2. \tag{29}$$

Resistivity ranges from 1000 to 150000 Rayls/m which corresponds to realistic values. By setting the porosity to $\phi = 0.9$, this allows the pore radius to vary between 34 and 402 μm.

Wave equation(s) and boundary conditions and radial modes

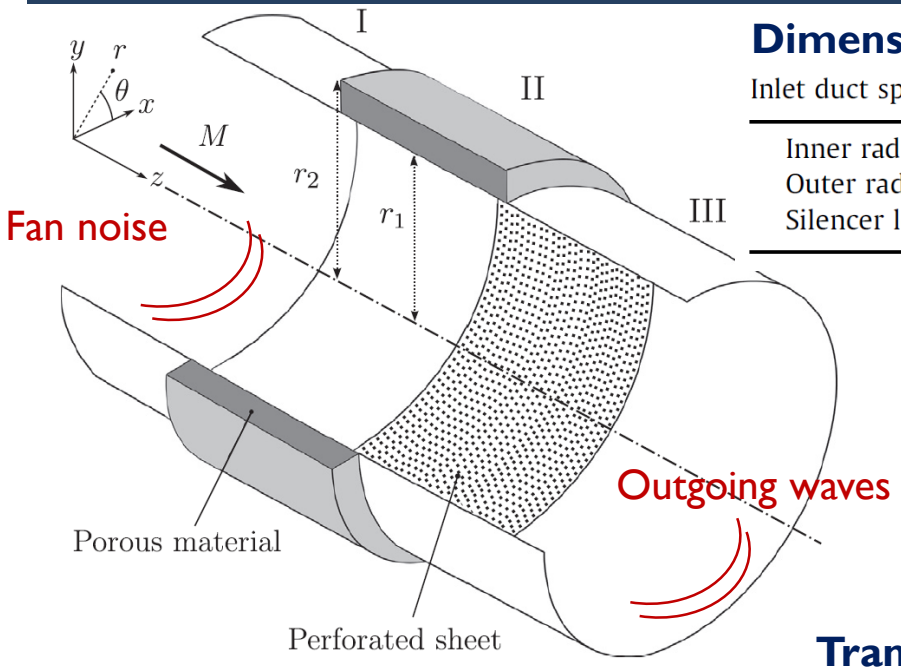

Fig. 1. Geometry of the silencer.

Dimensions

Inlet duct specifications with porous layer of thickness $h = r_2 - r_1 = 30$ mm.

Inner radius	r_1	0.99 m
Outer radius	r_2	1.02 m
Silencer length	L	0.66 m

Separation of variable

$$p(r,\theta,z,t) = p_{1,2}(r)\mathrm{e}^{i(m\theta+\beta z-\omega t)}$$

Convected Helmholtz equation

$$\frac{\mathrm{d}^2 p_1}{\mathrm{d}r^2} + \frac{1}{r}\frac{\mathrm{d}p_1}{\mathrm{d}r} + \left(\alpha_1^2 - \frac{m^2}{r^2}\right)p_1 = 0,$$

$$\frac{\mathrm{d}^2 p_2}{\mathrm{d}r^2} + \frac{1}{r}\frac{\mathrm{d}p_2}{\mathrm{d}r} + \left(\alpha_2^2 - \frac{m^2}{r^2}\right)p_2 = 0$$

$$\alpha_1^2 = k_1^2 - \beta^2(1-M^2) - 2k_1 M\beta,$$

$$\alpha_2^2 = k_2^2 - \beta^2,$$

Transmission conditions

$$p_1 - p_2 = -i\frac{\rho_1 Z}{\rho_2 k_1}\frac{\mathrm{d}p_2}{\mathrm{d}r}, \quad \text{at } r = r_1, \tag{5}$$

$$\rho_1\phi(M\beta - k_1)^2\frac{\mathrm{d}p_2}{\mathrm{d}r} = \rho_2 k_1^2\frac{\mathrm{d}p_1}{\mathrm{d}r}, \quad \text{at } r = r_1, \tag{6}$$

$$\frac{\mathrm{d}p_2}{\mathrm{d}r} = 0, \quad \text{at } r = r_2. \tag{7}$$

where Z is the dimensionless (with respect to the air characteristic impedance $\rho_1 c_1$) perforate plate impedance, ϕ is the open porosity and ρ_2 and c_2 are respectively, the equivalent density and the speed of sound in the porous material.

Mode calculation via Chebyshev interpolation

Chebyshev interpolation

$$(\beta^2 \mathsf{A} + \beta \mathsf{B} + \mathsf{C})\mathbf{p} = 0,$$

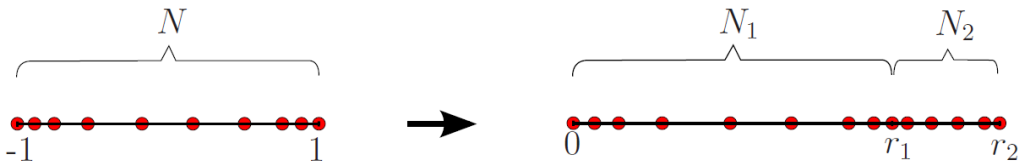

Figure 2: Distribution of Chebyshev points in each domain.

where $\mathsf{A}, \mathsf{B}, \mathsf{C}$ are square matrices and $\mathbf{p}$ contains the value of the acoustic pressure at the Chebyshev points for both domains. This quadratic problem is conveniently recast into the generalized eigenvalue problem

$$\begin{pmatrix} 0 & \mathsf{I} \\ \mathsf{C} & \mathsf{B} \end{pmatrix} \mathbf{X} = \beta \begin{pmatrix} \mathsf{I} & 0 \\ 0 & -\mathsf{A} \end{pmatrix} \mathbf{X} \quad \text{where} \quad \mathbf{X} = \begin{pmatrix} \mathbf{p} \\ \beta \mathbf{p} \end{pmatrix} \tag{11}$$

Computed eigenvalues are checked via dispersion equation

$$\begin{aligned} F_m(\beta) &= \rho_2 k_1^2 \alpha_1 \mathcal{J}_m^{11} (J_m(\alpha_2 r_1)\mathcal{Y}_m^{22} - Y_m(\alpha_2 r_1)\mathcal{J}_m^{22}) \\ &- \rho_1 \alpha_2 \phi (k_1 - M\beta)^2 J_m(\alpha_1 r_1)(\mathcal{J}_m^{21}\mathcal{Y}_m^{22} - \mathcal{Y}_m^{21}\mathcal{J}_m^{22}), \end{aligned}$$

MAPLE with arbitrary precision arithmetic

(m,n)	β_{mn}^+	$F_m^{\mathbf{40}}$	$F_m^{\mathbf{60}}$
(0,1)	$61.11556 + \mathrm{i}0.00075$	2.8	$9\,10^{-7}$
(3,1)	$60.63384 + \mathrm{i}0.00555$	0.8	$2\,10^{-7}$
(0,3)	$60.15811 + \mathrm{i}0.01070$	0.5	$3\,10^{-6}$
(4,2)	$59.48866 + \mathrm{i}0.01849$	0.01	$4\,10^{-7}$

Mode Matching Method

Mode expansion

$$p^i = \sum_{m=0,\pm1,\ldots} \sum_{n\geq 1} \left(A^{i+}_{mn} \Phi^{i+}_{p,mn} \mathrm{e}^{\mathrm{i}\beta^{i+}_{mn} z} + A^{i-}_{mn} \Phi^{i-}_{p,mn} \mathrm{e}^{\mathrm{i}\beta^{i-}_{mn} z} \right)$$

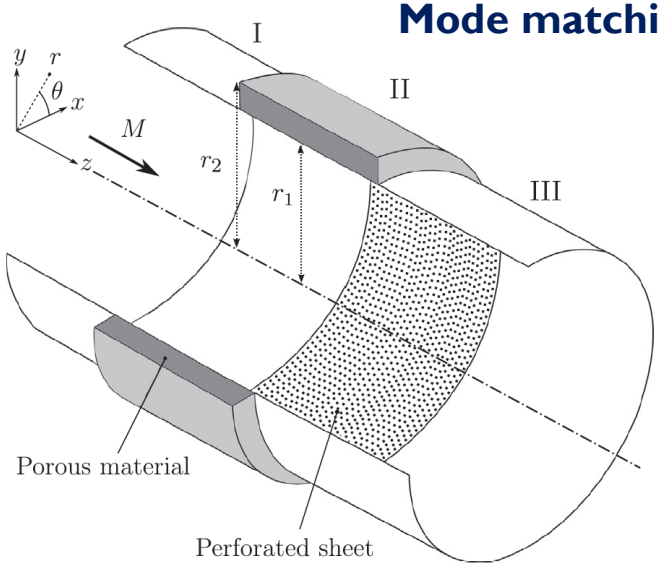

Fig. 1. Geometry of the silencer.

Mode matching at S_1 and S_2

Test function

$$\begin{aligned}
\int_{S_1} \Psi_p \, p^{\mathrm{I}} \mathrm{d}S &= \int_{S_1} \Psi_p \, p^{\mathrm{II}} \mathrm{d}S, \\
\int_{S_1} \Psi_w \, w^{\mathrm{I}} \mathrm{d}S &= \int_{S_1} \Psi_w \, w^{\mathrm{II}} \mathrm{d}S, \\
\int_{S_2} \Psi_w \, w^{\mathrm{II}} \mathrm{d}S &= 0.
\end{aligned}$$

Axial velocity

Scattering system

$$\mathsf{X}_1 \begin{pmatrix} \mathbf{A}^{\mathrm{I}-} \\ \mathbf{A}^{\mathbf{II}+} \end{pmatrix} = \mathsf{Y}_1 \begin{pmatrix} \mathbf{A}^{\mathrm{I}+} \\ \mathbf{A}^{\mathrm{II}-} \end{pmatrix}, \tag{20}$$

$$\mathsf{X}_2 \begin{pmatrix} \mathsf{E}^{\mathrm{III}+}(L) & 0 \\ 0 & \mathsf{E}^{\mathrm{II}-}(L) \end{pmatrix} \begin{pmatrix} \mathbf{A}^{\mathrm{III}+} \\ \mathbf{A}^{\mathrm{II}-} \end{pmatrix} = \mathsf{Y}_2 \begin{pmatrix} \mathsf{E}^{\mathrm{III}-}(L) & 0 \\ 0 & \mathsf{E}^{\mathrm{II}+}(L) \end{pmatrix} \begin{pmatrix} \mathbf{A}^{\mathrm{III}-} \\ \mathbf{A}^{\mathbf{II}+} \end{pmatrix}. \tag{21}$$

Transmission Loss for automative dissipative silencers (plane wave)

[4] B. Nennig, M. Ben Tahar, E. Perrey-Debain, A displacement-pressure finite element formulation for analyzing the sound transmission in ducted shear flows with finite poroelastic lining, The Journal of the Acoustical Society of America 130 (1) (2011) 42–51.

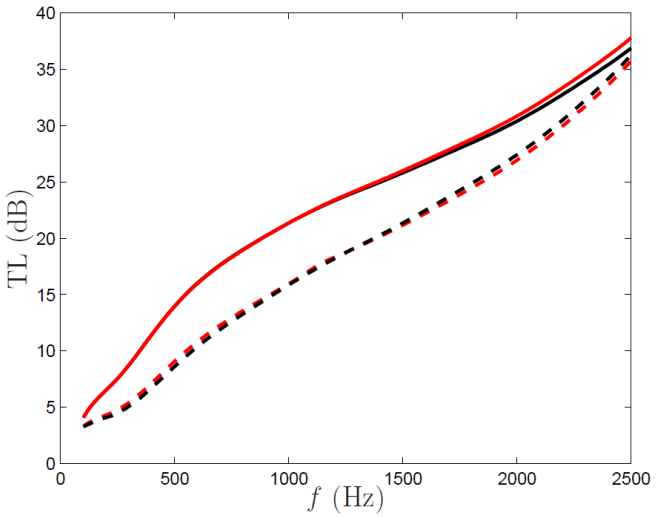

Figure 3: TL for the silencer described above with RGW2 wool; — MMM for $M = 0$; — 3D FEM for $M = 0$; – – MMM for $M = 0.2$; – – 3D FEM for $M = 0.2$.

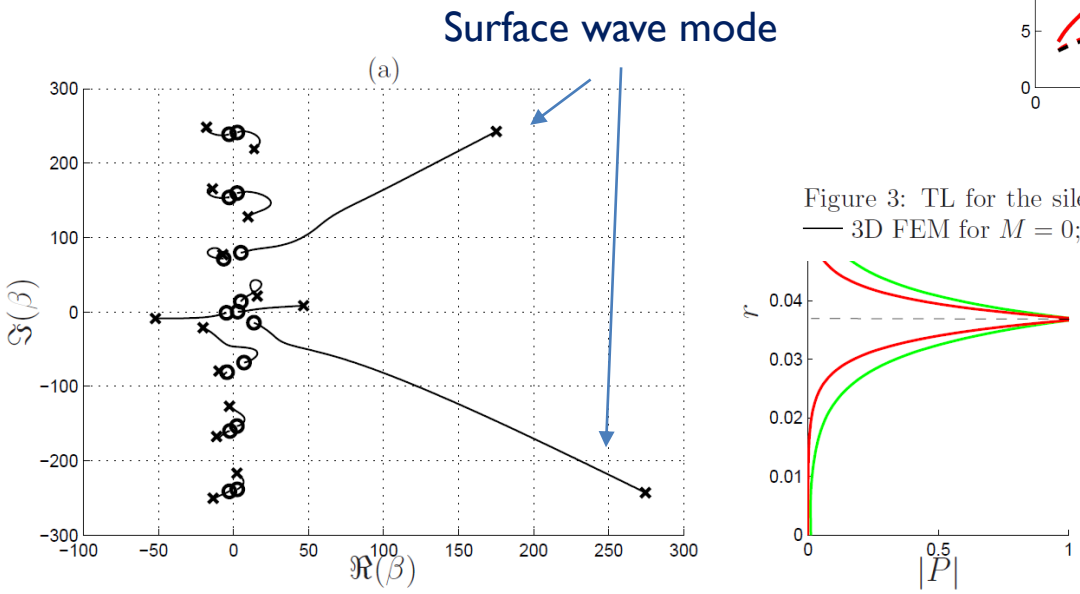

Figure 4: (a) Trajectories of the eigenvalues in the complex plane for the frequency ranging from 100(∘) to 2500Hz(×), treated with a RGW2 wool for $M = 0.2$; (b) Acoustic pressure mode shapes for positive (downstream) and negative (upstream) surface modes at 2500Hz.

Transmission Loss in a higly multimodal context

Incident field we follow standard assumptions often encountered in aeronautics, which mean that the incident sound field generated by the fan is decomposed as a set of modes $\mathbf{A}^{\mathrm{I}+}$ with random phase, and each azimuthal order carries the same power which is equally distributed over all the propagating radial modes.

$$\Phi^{i\pm}_{p,mn}(r,\theta) = N_{mn} J_m(\alpha_{mn} r/r_1)\, \mathrm{e}^{\mathrm{i}m\theta}$$

Transmission Loss

$$\mathrm{TL} = 10\log_{10}\frac{W^{\mathrm{I}+}}{W^{\mathrm{III}+}} = 10\log_{10}\frac{\sum' W^{\mathrm{I}+}_{mn}}{\sum' W^{\mathrm{III}+}_{mn}}, \qquad (22)$$

where symbol ($'$) signifies that only propagating modes are retained in the summation. The modal sound power is given by Joseph et al. [28]

$$W_{mn} = D_{mn}|A_{mn}|^2 \quad \text{where} \quad D_{mn} = \frac{\chi_{mn}(1-M^2)^2}{2\rho_1 c_1 (1-\chi_{mn}M)^2} \qquad (23)$$

Perf. Plate	POA (%)
P1	20
P2	10
P3	5

Transmission Loss, M=-0.5

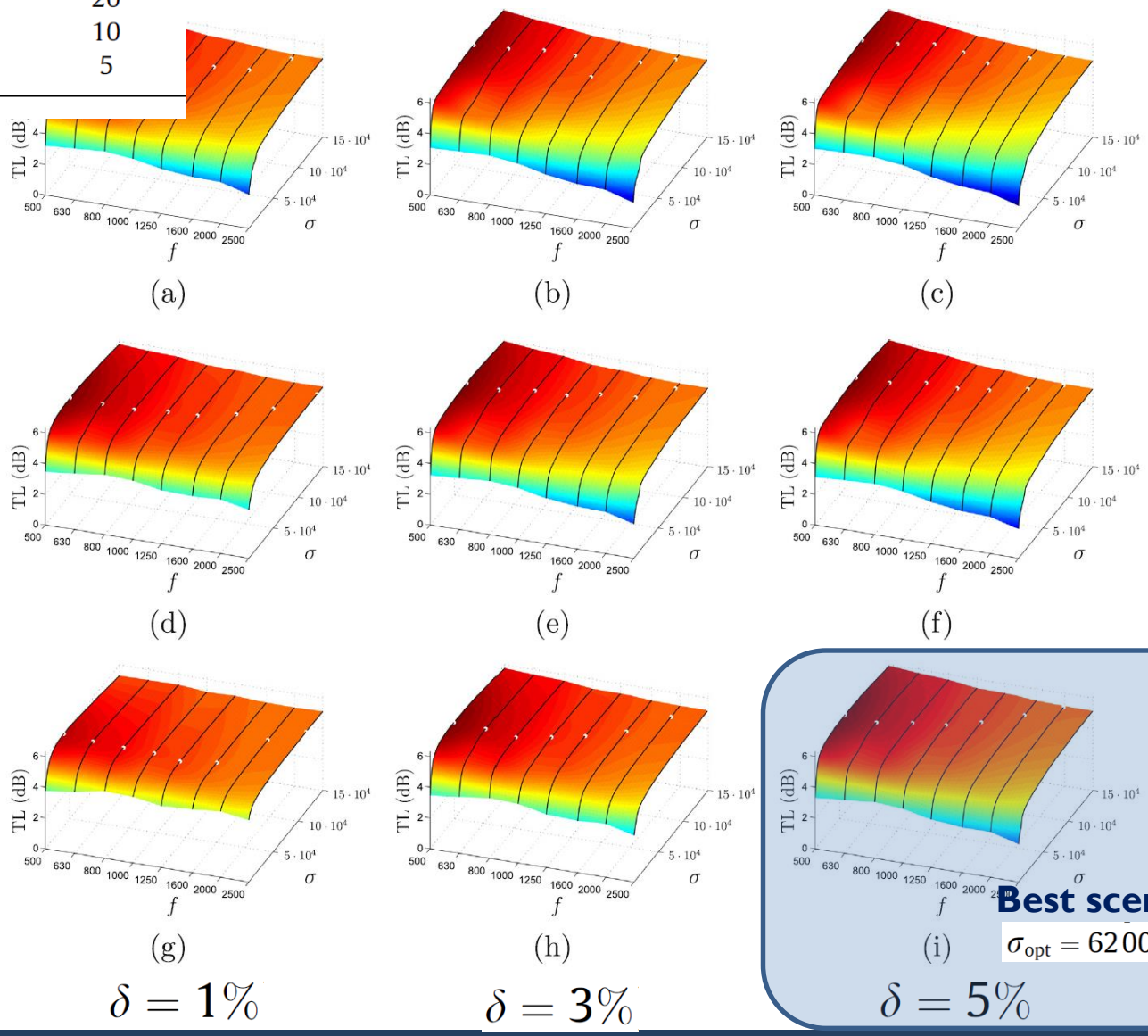

Comparison with DDOF liner (Snecma)

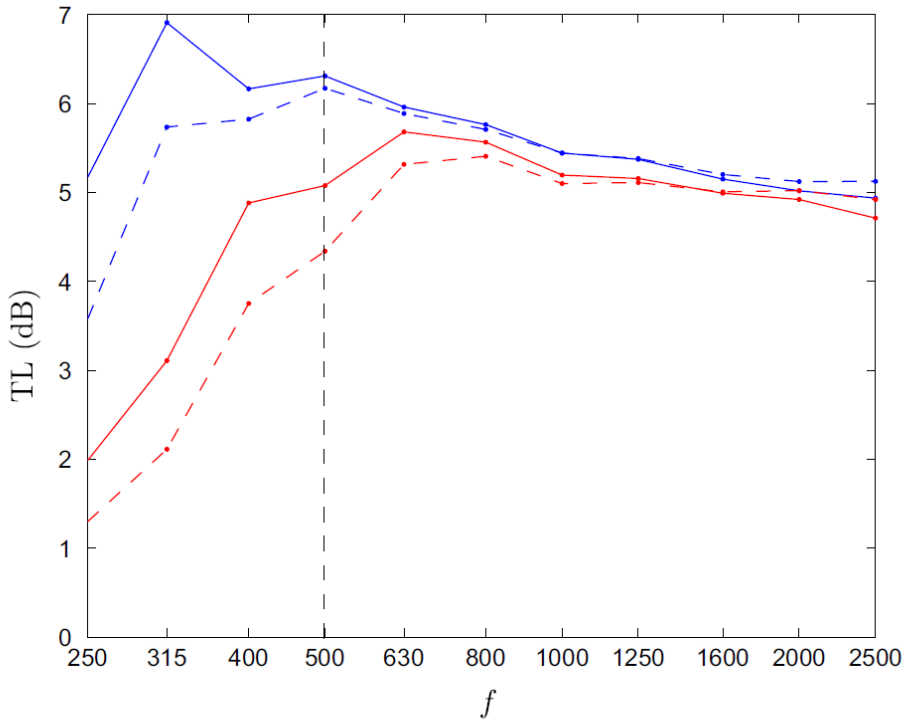

Fig. 4. Performance of the two optimal liners. Porous liner at Mach −0.3 (——), DDOF at Mach −0.3 (— —), Porous liner at Mach −0.5 (——), DDOF at Mach −0.5 (——)

Comparison with Actran (DDOF liner)

Predicted TL with an optimized DDOF liner (Snecma). Comparisons between the mode matching method and the finite element software Actran.

$M = -0.3$	500	630	800	1000	1250	1600	2000	2500
Mode matching	4.34	5.32	5.41	5.10	5.11	5.01	5.02	4.92
Actran	4.35	5.29	5.37	5.06	5.08	4.99	5.01	4.92
$M = -0.5$	500	630	800	1000	1250	1600	2000	2500
Mode matching	6.17	5.89	5.71	5.44	5.38	5.20	5.12	5.13
Actran	6.09	5.77	5.59	5.34	5.29	5.14	5.07	5.07

Comparison with DDOF liner (Snecma)

h	250	315	400	500	630	800	1000
20 mm	-1.00	-1.15	-0.50	-0.25	-0.10	-0.10	-0.10
25 mm	-0.95	-0.65	-0.20	-0.05	-0.05	-0.05	0.00
35 mm	0.65	0.25	0.10	0.05	0.00	0.00	0.00
40 mm	1.00	0.35	0.10	0.05	0.00	0.00	0.00

Table 2: Influence of the porous liner thickness on the performances, $M = -0.5$. Reported values correspond to the gain or loss (in dB) compared to the reference thickness $h = 30$ mm.

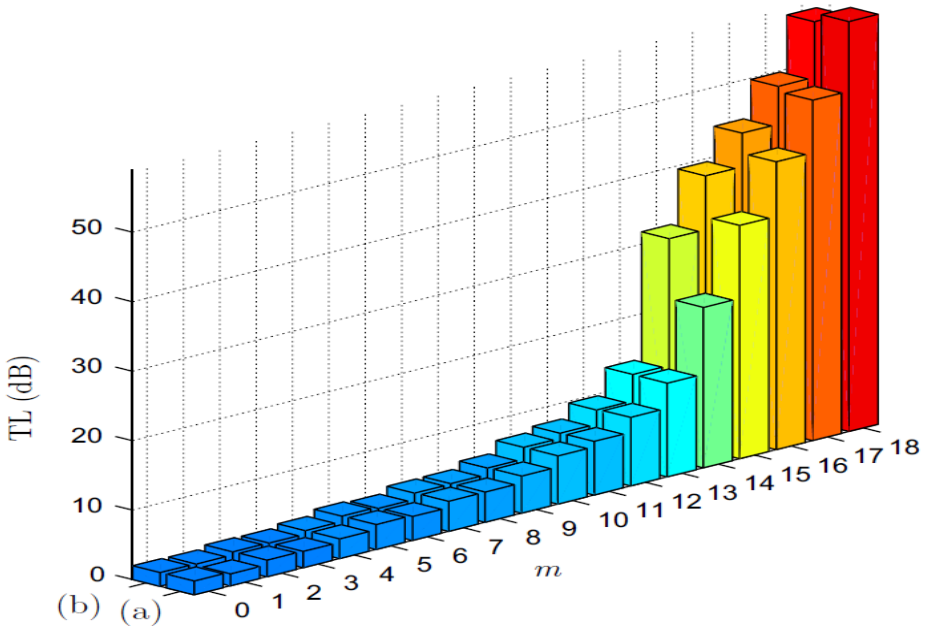

Fig. 5. Transmission loss with respect to azimuthal mode order at 1000 Hz: (a) Porous liner, (b) DDOF.

Conclusions

A parametric study that includes the most influential parameters, i.e.

- ❑ the resistivity of the foam and
- ❑ the resistance of the perforated sheet,

has been conducted in order to determine the optimal liner that maximizes the sound transmission losses. It is found that a large variety of porous liners are expected to produce similar performances as long as the airflow resistivity of the porous material is chosen sufficiently high (above 50000 Rayls/m) and the dimensionless resistance of the perforated plate should chosen be around the unity.

Comparisons with existing DDOF locally reacting acoustic liners show that, though performances are comparable, the presence of the metal foam has the potential to further reduce fan noise especially in the low frequency part of the spectrum, typically below 500 Hz. It would be interesting for future research to conduct real-scale experiments.